Current Research in Green and Sustainable Chemistry 4 (2021) 100099

Contents lists available at ScienceDirect

Current Research in Green and Sustainable Chemistry

journal homepage: www.elsevier.com/journals/current-research-in-green-and-sustainable-chemistry/2666-0865

Fabrication and electrochemical performances of SnO_2@C composite materials

Shangkun Wang [a,b], Guiying Xu [a,b,**], Kun Wang [a,b,***], Beibei Han [d], Yingxin Wang [c], Lixiang Li [a,b], Dongying Ju [d], Maorong Chai [d], Dakui Zhang [a,b], WeiMin Zhou [a,b,*]

[a] Key Laboratory of Energy Materials and Electrochemistry Research Liaoning Province, University of Science and Technology Liaoning, Anshan 114051, PR China
[b] Ansteel Chemical Co., Ltd, No.1 Huangang Road, Tiexi District, Anshan City, Liaoning Province, China
[c] JiXi Weida New Material Technology Co., Ltd, No 8, Lexin Street, Jiguan Industrial Park, Jixi City, Heilongjiang Province, China
[d] Advanced Science Research Laboratory, Saitama Institute of Technology, 1690 Fusaiji, Fukaya, Japan

ARTICLE INFO

Keywords:
SnO_2 compound
Metal oxides
Lithium ion batteries (LIBs)
SnO_2@C composite materials

ABSTRACT

SnO_2@C composite materials are facilely fabricated by reaction using the gelatin, $SnCl_4$•$5H_2O$ and aqueous NH_3•H_2O by one-step method. Compared to the SnO_2, the prepared SnO_2@C composite materials show the fabulous improvement about rate performances and cycling performances, when controlling the carbon contents of carbon in SnO_2@C composite materials. As an example, SnO_2@C-40 shows the cycling performance at 397.7 mAh/g, after carrying out the charge-discharge cycles 500 times at 0.1 A/g. These ameliorated electrochemical performances lead us to consider our provided preparation method is the efficient way to facilitate the application of SnO_2@C in fabrication of lithium ion batteries (LIBs) as negative electrode materials.

1. Introduction

To address the problem regarding to the greenhouse gas emissions, the unfolding of electric vehicle (EV) is extensively encouraged in the world. Therefore, the development of researches about electrodes of LIBs becomes extremely popular [1]. In particular, the developments about negative materials are exceedingly active than ever before.

Recently, to obtain the negative materials having high storage capacity, a large number of researchers pour attention to the transition metal oxides such as Fe_2O_3, Fe_3O_4, FeO, SnO_2 and MnO_2 because they have the high theoretical capacity [2–5]. Thereinto, SnO_2 has been intrigued significantly because the SnO_2 possesses the high theoretical capacity and relatively low cost [6,7].

It is well known that volumetric expansion problem restricts the cycling performances of transition metal oxide materials. Similarly, it is unavoidable that this problem also restricts the application of SnO_2 as electrode materials. Thus, a lot of methods are unfolded to solve aforementioned anguish problem about application of SnO_2. For instance, it is aware of that making the SnO_2 to possess nano size is more effective way to overcome the volumetric expansion of SnO_2 [8]. Additionally, covering the carbon materials on the surface of SnO_2 is another general effective method to enhance the electrochemical performances of SnO_2 because the carbon materials can increase the conductivity not only, but also can restrict the volumetric expansion of SnO_2 [9–11].

Gelatin as carbon source is widely utilized to cover the metal oxides to restrict their volumetric expansion by now, for the gelatin possesses a plenty of organic groups which can remarkably facilitate the metal oxide compounds disperse in it [12–14]. On the basis of industrialization viewpoint, we attempt to use the gelatin as carbon source to cover the metal oxide compounds by one step method. In our presented studies, the Fe_7S_8@C composite materials were prepared successfully, and its excellent electrochemical performances were described [14].

Likewise, in order to expand SnO_2 in actual application to fabricate electrodes, we also performed the preparation of SnO_2@C materials by one stage method that $SnCl_4$•$5H_2O$ directly reacted with the aqueous NH_3•H_2O and gelatin. As a result, it is observed that the SnO_2 in

* Corresponding author. Key Laboratory of Energy Materials and Electrochemistry Research Liaoning Province, University of Science and Technology Liaoning, Anshan 114051, PR China.
** Corresponding author. Key Laboratory of Energy Materials and Electrochemistry Research Liaoning Province, University of Science and Technology Liaoning, Anshan 114051, PR China.
*** Corresponding author. Key Laboratory of Energy Materials and Electrochemistry Research Liaoning Province, University of Science and Technology Liaoning, Anshan 114051, PR China.
E-mail address: aszhou15242870697@163.com (W. Zhou).

https://doi.org/10.1016/j.crgsc.2021.100099
Received 21 December 2020; Received in revised form 22 March 2021; Accepted 28 March 2021
Available online 2 May 2021

amorphous state exists in SnO_2@C composite materials, which was verified by measurements of X-ray diffraction (XRD) and transmission electron microscope (TEM).

Compared to the SnO_2, the SnO_2@C composite materials exhibit the remarkable improvement about electrochemical performances, indicating that one stage method using the gelatin as carbon source to cover the SnO_2 is also effective way to enhance the electrochemical performances of SnO_2.

2. Experimental

2.1. Characterization

The measurements of XRD were carried out by X'pert Powder instrument from PANalytical, Holland. Scanning electron microscope (SEM) morphologies were evaluated by instruments of Carl Zeiss AG, Germany and Apreo, FEI Ltd., USA. Thermogravimetric analysis (TGA) was performed by thermal gravimetric analyzer (TG209F3) of NETZSCH Group, Germany. The X-ray photoelectron spectroscopy (XPS) measurements were carried out by Axis Ultra DLD instrument of Kratos, UK. Nitrogen adsorption and desorption isotherm was measured by Quadrasorb autosorb-iQ surface analyzer which was purchased from Quantachrome Instruments, USA. Specific surface area was determined in detail, according to the BET method. The pore size distribution was assessed by BJH model for slit pores. Electrochemical measurements were performed by the electrochemical system (CHI660E) of ChenHua, Shanghai, China. Table type high speed centrifuge was purchased from Shanghai Fichal Analytical Instrument Co., Ltd., China. TEM measurements were carried out by the HF-3300 Hitachi, Ltd., Japan.

2.2. Preparation of SnO_2 nanospheres

On the basis of report by Mohanta et al. the SnO_2 nanospheres were prepared successfully [15]. The $SnCl_4{\bullet}5H_2O$ (0.35 g) was dissolved in the deionized water (40 mL). The $NH_3{\bullet}H_2O$ (4 M) was dripped into the solution containing the $SnCl_4{\bullet}5H_2O$ until the pH value became the 7. It is found that the white solids clearly formed with stirring the obtained mixture solution for 1 h. After filtration, the white solids were obtained and respectively washed by deionized water and anhydrous alcohol with three times. Finally, after the obtained solids had been dried at 80 °C for 12 h and then treated at 500 °C for 3 h in air, the SnO_2 nanospheres were obtained successfully.

2.3. Preparations of SnO_2@C composite materials

Firstly, the gelatin (10 g) was dissolved in the deionized water (90 mL) at 80 °C, and the obtained solution was uniformly stirred with the 300 r/min. As a result, the gelatin solution with light yellow colour was obtained and named **α**. Thereafter, the $SnCl_4{\bullet}5H_2O$ (0.35 g) was respectively dissolved in the deionized water (40 mL) with stirring for 0.5 h in the three beakers, and the colourless transparent solution were obtained and named as **β** solution.

Continuously, the ***α*** solutions owning the volumes of 15 mL, 40 mL and 90 mL were respectively added into the **β** solution. After stirring the obtained mixture solutions for 30 min, the $NH_3{\bullet}H_2O$ (4 M) was dripped into the solution until the pH value became around 7. The obtained solutions were stirred at 60 °C until they became the milk white suspensions. After cooling the reaction cases to room temperature, the white solids in gel state were obtained.

The obtained white solids were dried in the oven at 80 °C for 16 h, and then obtained solids were ground into powders. The powders were placed in the furnacetube, and treated at 500 °C for 3h in N_2. After cooling the solids to the room temperature, the products were obtained and named as SnO_2@C-15, SnO_2@C-40 and SnO_2@C-90, respectively, according to the usage of volumes of gelatin solutions (**α**).

2.4. Electrochemical measurements

The electrochemical cells were assembled using the SnO_2@C composite materials. Firstly, SnO_2@C composite materials (0.08 g) were respectively mixed with acetylene black (0.01 g) and polyvinylidine fluoride (PVDF) binder (0.01 g) in a weight ratio of 80:10:10 in N-methyl-2-pyrrolidone (NMP) solution. The obtained slurry was coated on the Cu foil and dried in vacuum drying oven at 80 °C for 1 h to remove solution. Subsequently, the Cu foil with the active materials were dried at 120 °C for 12 h in the same vacuum drying oven and cut into round shape strips of ϕ 11 mm in size. The mass loading of the active materials was controlled at 1.20 mg/cm^2. The two-electrode electrochemical cells (CR2032 coin-type) were assembled in a glove box filled with high-purity argon, in which cells were assembled using the lithium metal foil (ϕ 15.60 mm × 0.45 mm) as reference electrode, Celgard 2400 microporous membrane as separator, and 12–13 wt% of $LiPF_6$ in the mixture of EC, DMC, EMC (1:1:1, vol%) as electrolyte. Galvanostatic charge-discharge test was carried out by LAND (CT 2001A) battery test system in the voltage range of 0.05–3.00 V. The same electrochemical cells were also used to carry out measurements of cyclic voltammetry (CV). CV and electrochemical impedance spectroscopy (EIS) measurements were carried out using the CHI 660E. The CV curves were recorded in the voltage region of 0.05–3.00 V at scan rate of 0.2 mV/s. The impedance spectra were recorded in a frequency range of 100 kHz - 0.01 Hz, and the amplitude was 5 mV.

3. Results and discussion

Firstly, the carbon contents covered on the surface of SnO_2 were investigated by TGA measurements in air. As shown in Fig. S1, the prepared SnO_2@C-15, SnO_2@C-40 and SnO_2@C-90 manifested the weight loss before 300 °C, which was spontaneously attributed to the loss of water [16,17]. The intense weight loss in the temperature range of 300–600 °C was ascribed to the burning of the carbon materials [18]. Finally, based on the residual quantity of SnO_2, the carbon contents of SnO_2@C-15, SnO_2@C-40 and SnO_2@C-90 were respectively calculated at 62.0%, 68.2% and 74.2%.

The morphologies of SnO_2 nanospheres and SnO_2@C composite materials were evaluated by SEM measurements. Similarly, it is also observed that nano sphere SnO_2 particles were successfully prepared in our studies (Fig. 1a–b). In contrast, the morphologies of SnO_2@C composite materials showed the irregular blocky shapes, which were entirely different from the SnO_2 nanospheres (Fig. 1c–d). After the evaluations of EDS, it was evident that C, N, O, Sn elements exist on the surface of SnO_2@C composite materials (Fig. S2).

The elements on the surface of SnO_2@C composite materials were investigated by XPS measurements in detail. Firstly, the peaks of C1s, O1s and N1s were observed at 284.9 eV, 532.0 eV, 398.7 eV, respectively (Fig. 2a). To amply investigate the compounds on the surface of SnO_2@C composites, the aforementioned pecks were specifically analyzed. For instance, the C1s peak was fitted to the four peaks that are attributed to the C–C bound (284.7 eV), C–O (285.7 eV), C═O (287.8 eV) and C–O–O (289.0 eV), respectively (Fig. 2b). The peaks of 487.0 eV and 495.5 eV that are attributed to the $Sn3d_{5/2}$ and $Sn3d_{3/2}$ were observed respectively (Fig. 2c). The energy difference between the $Sn3d_{5/2}$ and $Sn3d_{3/2}$ is 8.5 eV which coincides with the characterization of Sn^{4+} existing in SnO_2@C composite materials [19]. Additionally, it was distinctly observed that N1s was able to be fitted four peaks such as 398.6 eV, 400.0 eV, 401.1 eV and 403.2 eV which correspond to the pyridinic N, pyrrolic-N, graphitic-N and oxide-N, respectively (Fig. 2d) [20]. It is naturally considerable that nitrogen elements brought by gelatin can improve the conductivity of SnO_2@C composites.

The structures of SnO_2@C composite materials were further verified by XRD measurements (Fig. 3). It was found that the four peaks of 27°, 34°, 38° and 52° that are respectively ascribed to the four lattice planes of (110), (101), (200) and (211) of SnO_2 crystal (Fig. 3a) [21,22]. In

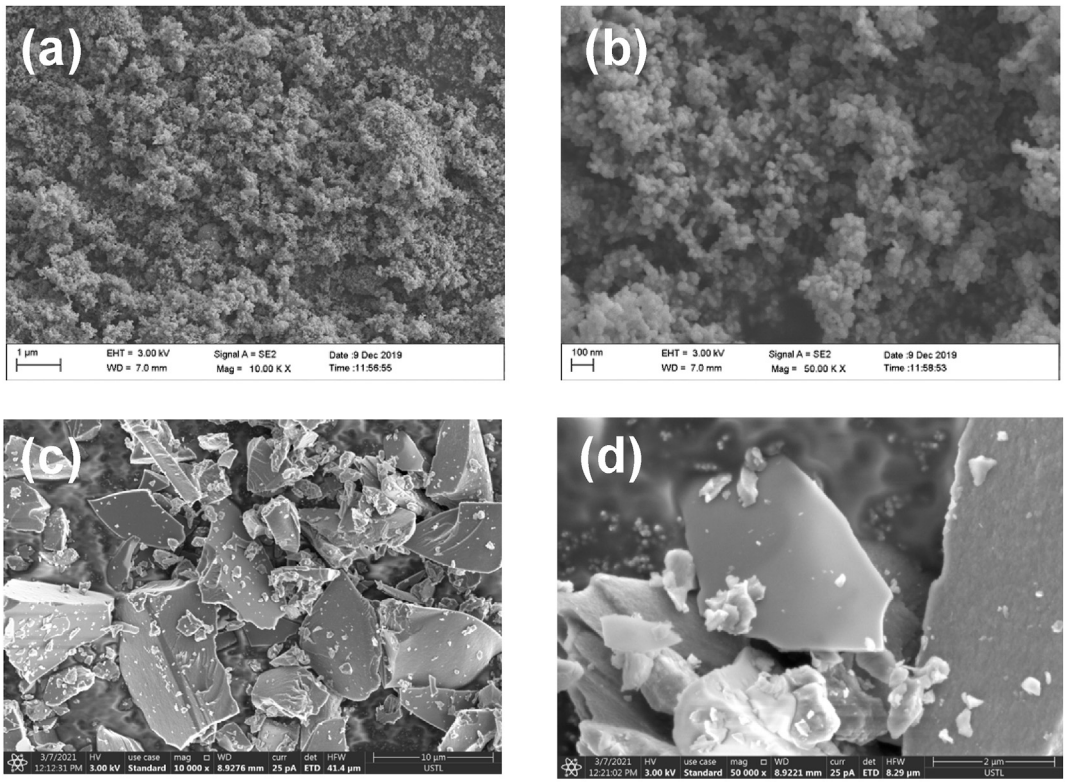

Fig. 1. (a) and (b) show the SEM morphologies of SnO_2, (c) and (d) exhibit the SnO_2@C-40 composite materials.

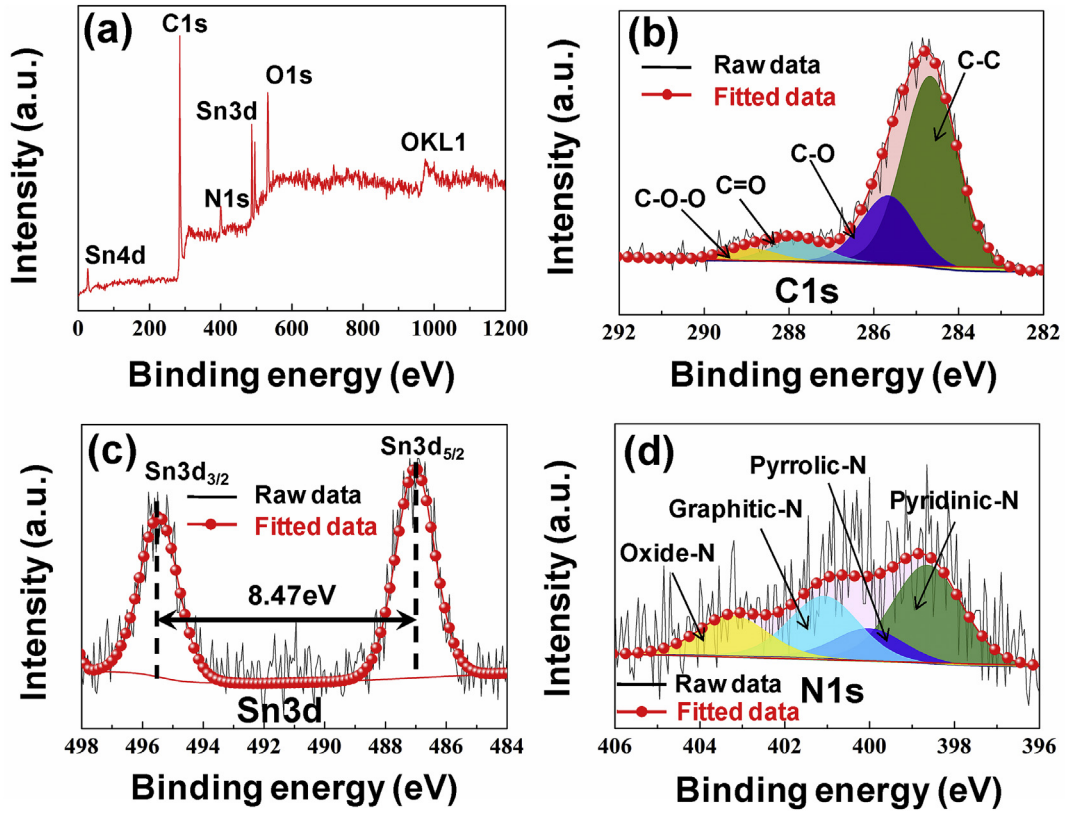

Fig. 2. XPS results of SnO_2@C-40.

accordance with the standard card as ICOD 01-077-0448 (Fig. 3b), it is clearly indicative of that the SnO_2 particles were prepared successfully. However, the characteristic peaks of SnO_2 were not expressly verified in SnO_2@C composite materials, leading us to consider that SnO_2 with

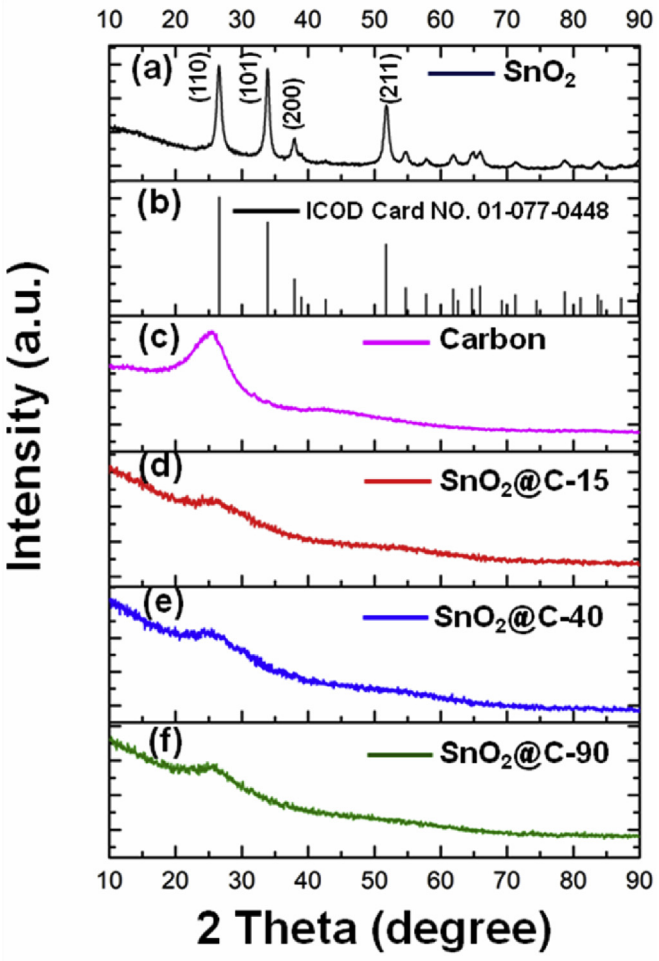

Fig. 3. XRD results of samples.

amorphous state mainly exists in SnO_2@C composite materials (Fig. 3d–f).

In addition, to investigate the detailed structures of SnO_2@C composite materials, the TEM measurements were performed in detail. It was obvious that the SnO_2 having slight agglomeration phenomenon dispersed in the carbon materials (Fig. 4a). Fig. 4b reveals that SnO_2@C composite materials mainly are the amorphous state. However, similar to the report by Li et al. it is evident that the SnO_2 having microcrystal structures partly exist in SnO_2@C composite materials [23]. As shown in Fig. 4C, we calculated their lattice distances of d_1, d_2 and d_3 at 0.34 nm, 0.33 nm and 0.27 nm, which corresponded to the three lattice planes of SnO_2 such as (110), (110) and (101), respectively (Fig. S3) [24]. These results provide another evidence for indicating the fact that SnO_2 exist in the SnO_2@C-40 composite materials.

The BET methods were used to investigate the conversions of surfaces and structures of SnO_2@C composite materials. Compared to the SnO_2@C-15 and SnO_2@C-90, the relatively big mesoporous (12.3 nm) appeared in the SnO_2@C-40 (Fig. S4). Additionally, SnO_2@C-40 exhibited the relatively bigger specific surface area than the SnO_2@C-15 and SnO_2@C-90 (Table S1). These results reveal that controlling the carbon contents in SnO_2@C composite materials also could converse their structures remarkably.

According to the general evaluation methods, the electrochemical performances of SnO_2@C composite materials were evaluated systematically [25]. Fig. 5a illustrated the cycle performances of carbon, SnO_2 and SnO_2@C composite materials. In comparisons with carbon and SnO_2, the SnO_2@C composite materials manifested the noticeable improvement of cycle performances. After carrying out charge-discharge 100 times, the SnO_2@C-15, SnO_2@C-40 and SnO_2@C-90 showed the Li^+ ion storage capacity at 321.9 mAh/g, 353.6 mAh/g and 307.9 mAh/g, respectively, which were extremely higher than the 57.8 mAh/g of SnO_2 and 111.9 mAh/g of carbon materials (obtained from carbonization of gelatin). Especially, the Li^+ storage capacity of SnO_2@C-40 was increased to the 397.7 mAh/g, after the charge-discharge processes were carried out 500 times (Fig. 5C). It was also observed that SnO_2@C-40 displayed the analogous cycling performance behavior, similar to presented reports [26,27]. Namely, when conducting the charge-discharge 154 times, the Li^+ storage capacity began to exhibit the increased tendency until the charge-discharge was carried out 500 times. This phenomenon is presumably ascribed to the influence of reversible formations of polymeric gel-like film on the surface of SnO_2@C-40.

The evaluations about the rate performance results are showed in Fig. 5b. After carrying out the charge-discharge 10 times at different current densities such as 0.1 A/g, 0.2 A/g, 0.5 A/g, 1.0 A/g, respectively, the SnO_2@C-40 showed the Li^+ storage capacity at 385.3 mAh/g when the current density recovered to the 0.1 A/g again. By contrast, the SnO_2, SnO_2@C-15 and SnO_2@C-90 respectively displayed the storage capacity at 50.5 mAh/g, 274.6 mAh/g, 322.6 mAh/g, when the current density recovered to the 0.1 A/g again. These results revealed that SnO_2@C-40 possessed the more tremendous rate performances than SnO_2, SnO_2@C-15 and SnO_2@C-90, respectively.

The charge-discharge properties of SnO_2 and SnO_2@C materials were displayed as shown in Fig. 6. The coulombic efficiencies of SnO_2, SnO_2@C-15, SnO_2@C-40 and SnO_2@C-90 were exhibited at 49.6%, 54.5%, 51.0% and 73.3% on the first cycle, and recovered to 100% after second cycle. In general, the coulombic efficiencies after second cycle are improved by the formation of SEI to prevent electrolyte decomposition. In comparison with the fact that charge-discharge plateau was observed in SnO_2, the similar charge-discharge plateaus were inconspicuously found in the SnO_2@C composite materials, which is attributed to their principal amorphous structures.

As shown in Fig. 7a–d, the reduction potentials were detected at 0.51 V, 0.64 V, 0.63 V and 0.63 V respectively on the first cycle, which were generally assigned to the formation of solid electrolyte interphase (SEI)

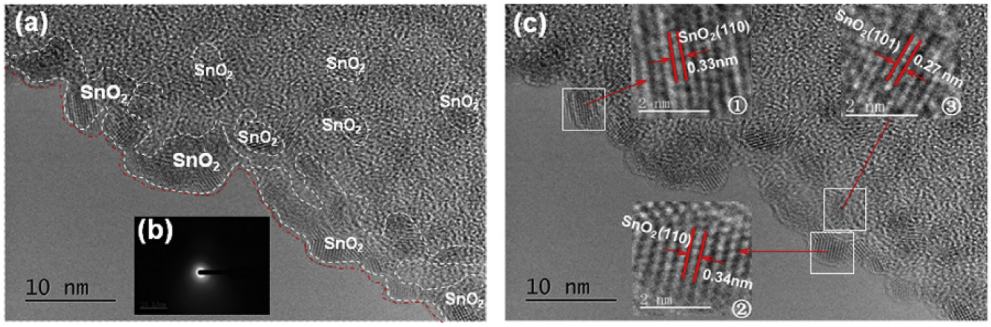

Fig. 4. TEM analyses about SnO_2@C composite materials. b) is the image of the selected area electron diffraction (SAED). c) is the magnified image of (a).

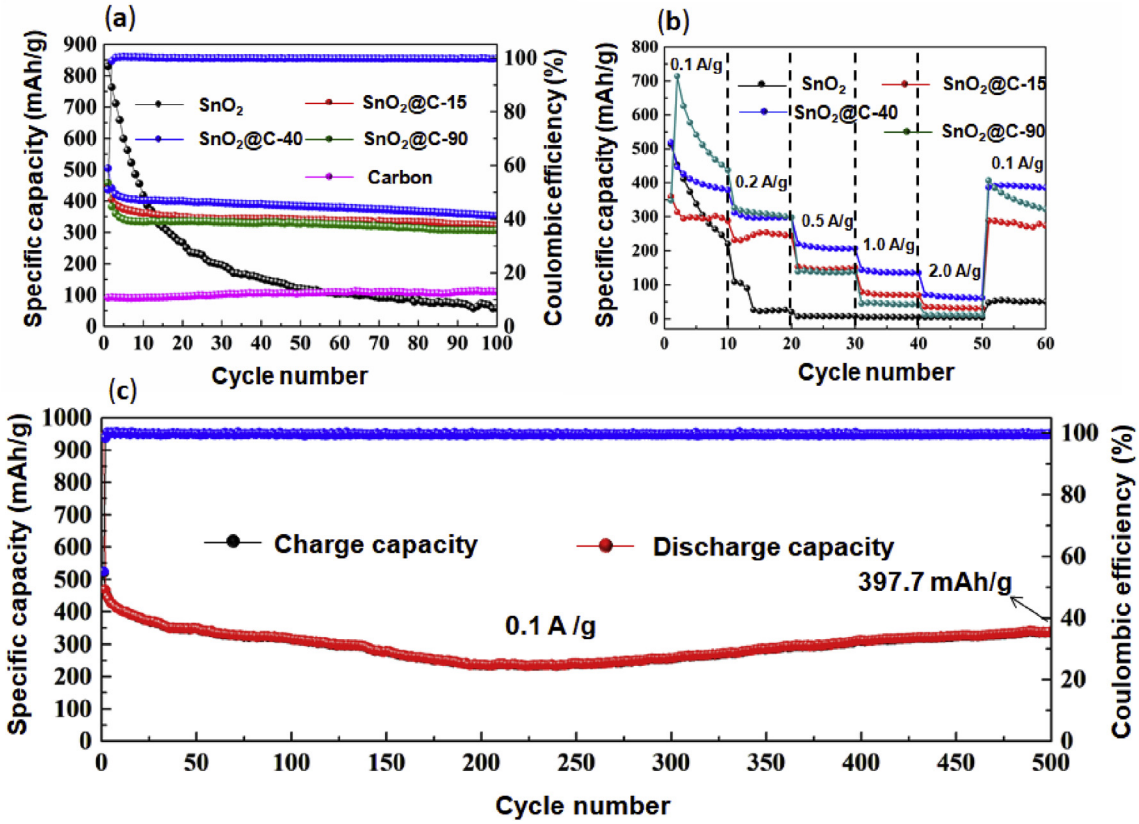

Fig. 5. Cycling performances (a) and Rate performances (b) of samples illustrated. (c) displays the cycling performances of SnO_2@C-40, after carrying out the charge-discharge 500 times.

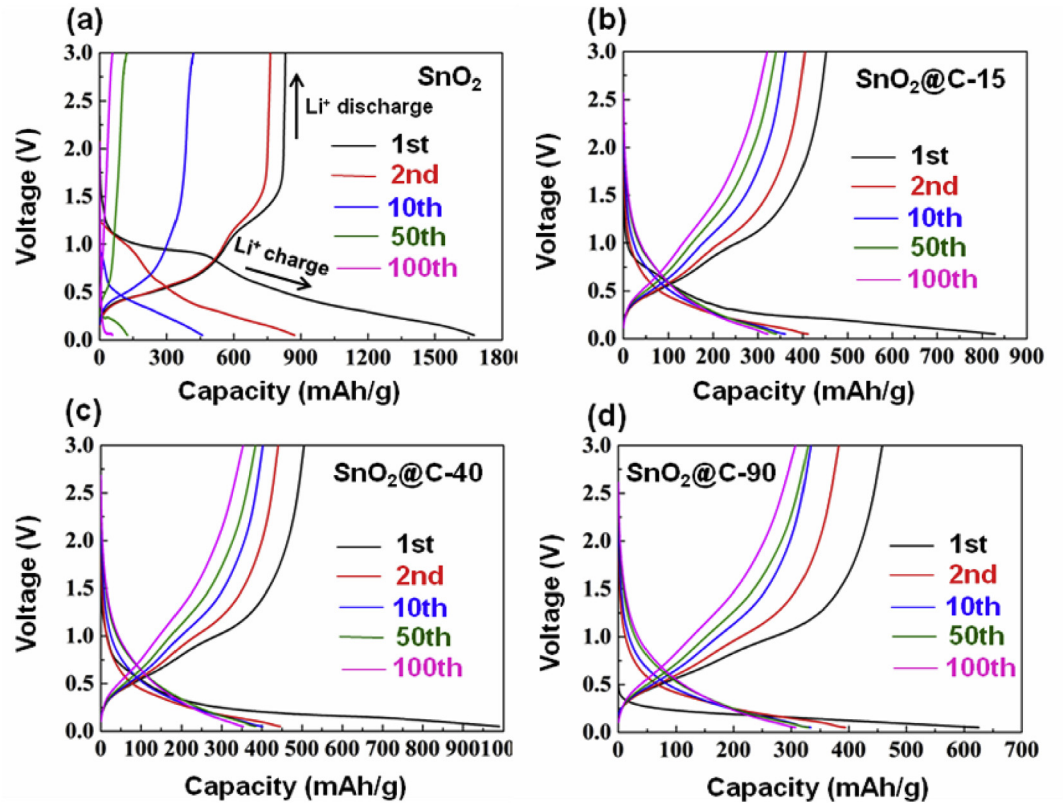

Fig. 6. Charge-discharge performances of SnO_2 (a), SnO_2@C-15 (b), SnO_2@-40 (c) and SnO_2@-90 (d).

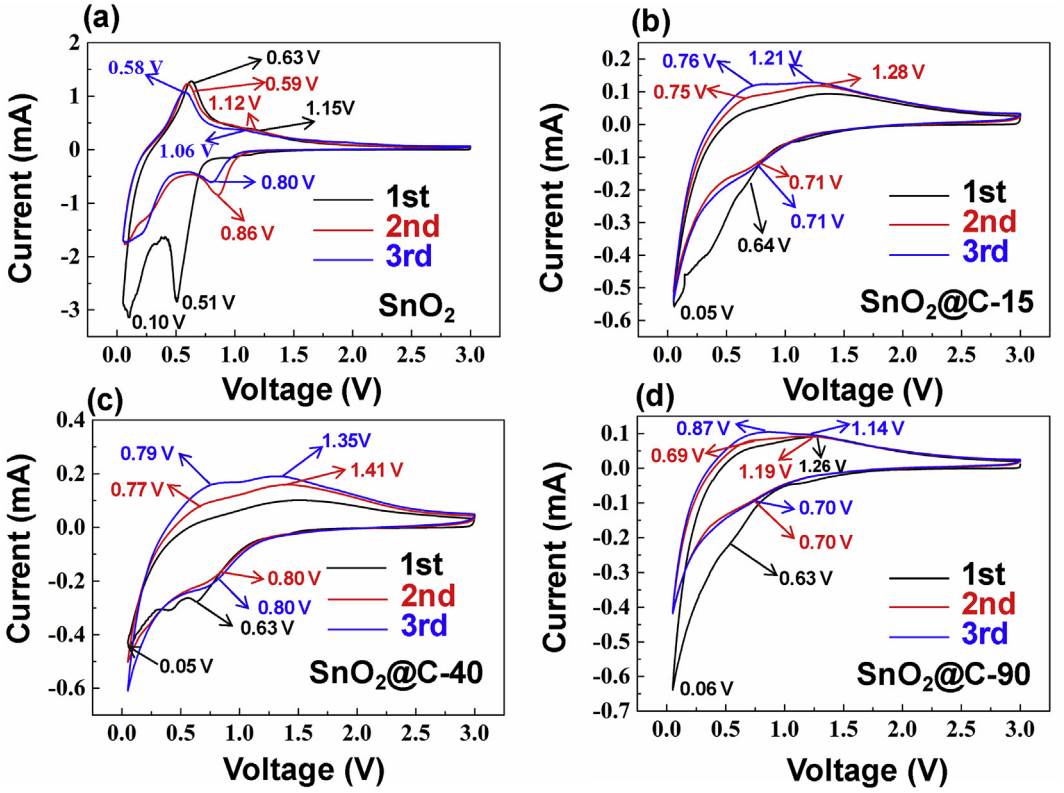

Fig. 7. CV measurements of SnO_2 (a), SnO_2@C-15 (b), SnO_2@C-40 (c) and SnO_2@ C-90 (d) at scan rate as 0.2 mV/s.

[28]. According to the report by Kisu et al. the reductive peaks of 0.10 V, 0.05 V, 0.05 and 0.06 V on first cycle were considered to the alloying reaction of Sn with Li^+. The de-alloying reaction peak of Li_xSn of SnO_2 was observed at 0.63 V, and the peak attributing to the oxidation (Sn was oxidized to the SnO_2) was observed at 1.15 V (Fig. 7a) [29]. By contrary, the SnO_2@C-15, SnO_2@C-40 and SnO_2@C-90 did not clearly show the de-alloying peaks on the same first cycles (Fig. 7b–d). Concurrently, the SnO_2@C-15, SnO_2@C-40 did not show the peak about oxidation that Sn was oxidized to the SnO_2, but this oxidation peak could be detected at 1.26 V in SnO_2@C-90 on the same first cycle (Fig. 7b–d) [30].

On the other hand, it was clarified that SnO_2@C-15, SnO_2@C-40 and SnO_2@C-90 respectively showed the de-alloying peaks at 0.75 V, 0.77 V and 0.69 V on the second cycle (Fig. 7b–d). Meanwhile, on the same second cycle, the peaks that Sn was oxidized to SnO_2 could be detected at 1.12 V, 1.28 V, 1.41 V and 1.19 V, respectively (Fig. 7a–d) [30]. Furthermore, similar to the SnO_2 particles, the slightly shifting of potentials about the aforementioned de-alloying and oxidation peaks of SnO_2@C composite materials was also observed on the third cycle, indicating that SnO_2@C composite materials possess the imperfect reversibility, which probably contributed to that SnO_2 having amorphous state exists in the SnO_2@C composite materials [31]. On the other side, it was observed that the peaks about the SEI did not show the obviously changing in the third cycle (Fig. 7b–d).

Fig. 8 manifested the electrochemical research-impedance results of SnO_2@C composite materials. As per the report by Wang et al. the EIS measurements were performed after charge-discharge 10 cycles [32]. As a result, the diameter of the semicircle of negative electrodes of SnO_2@C-40 was much smaller than that of SnO_2, SnO_2@C-15 and SnO_2@C-90. Meanwhile, the impedances of SnO_2, SnO_2@C-15, SnO_2@C-40 and SnO_2@C-90 were calculated at 123.0 Ω, 281.9 Ω, 20.9 Ω and 99.9 Ω, respectively (Fig. 8a, Table S2) [33,34]. On one hand, the kinetic differences between SnO_2, SnO_2@C-15, SnO_2@C-40 and SnO_2@C-90 were further confirmed by σ value of Warburg coefficient in Fig. 8b. The σ value could be obtained by measurement of the Randles plot which is plotting of Z′ with $\omega^{-1/2}$ ($\omega = 2\pi f$) for a low-frequency [35,36]. Larger value of σ is able to reflect the poor ion diffusion performance. As a result, the σ corresponding values of SnO_2, SnO_2@C-15, SnO_2@C-40 and SnO_2@C-90 were respectively calculated at 848.1 Ω $s^{-1/2}$, 133.1 Ω $s^{-1/2}$, 44.0 Ω $s^{-1/2}$ and 412.8 Ω $s^{-1/2}$, indicating that the SnO_2@C-40 possessed the remarkably higher Li^+ transfer than SnO_2, SnO_2@C-15, SnO_2@C-40 and SnO_2@C-90. These aforementioned results indicated that SnO_2@C-40 electrode possesses lower charge-transfer impedances than other materials, corresponding to the tendency of measurement results of rate performances.

BET results can explain the reason that SnO_2@C-40 owns the excellent Li^+ transfer because the SnO_2@C-40 possessed the relatively bigger porous structures than others (Fig. S4). Moreover, associating with the TGA results (Fig. S1), these results also are suggestive of that exceedingly improved conductivity naturally linked to the suitable carbon contents in SnO_2@C-40 composite materials.

Finally, in view of the reports by Wang et al. we investigated the storage mechanism by the dynamic analysis based on the CV curves at scan rates from 0.2 mV/s to 5.0 mV/s [37]. According to the dynamic analysis using CV measurement results at sweep rate of 2 mV/s, the SnO_2@C-40 shows the relatively capacitive contribution at (55.4%) which is higher than SnO_2@C-15 (52.7%) and SnO_2@C-90 (52.2%) (Fig. 9). Indeed, the SnO_2@C-40 also shows the higher capacitive contribution than SnO_2@C-15 and SnO_2@C-90 at other scan rates. These results reveal that increased capacitive contribution plays the role to improve storage capacity of SnO_2@C-40 (Fig. S5). At the present stage, we infer that SnO_2 having the microstructures in SnO_2@C composite materials probably play the rule to enhance the pseudocapacitance effect, which leads to the enhancing of capacitive effect [38].

4. Conclusions

The storage capacity of SnO_2 is successfully enhanced by covering the carbon materials on its surface. It is aware of that one-step method using

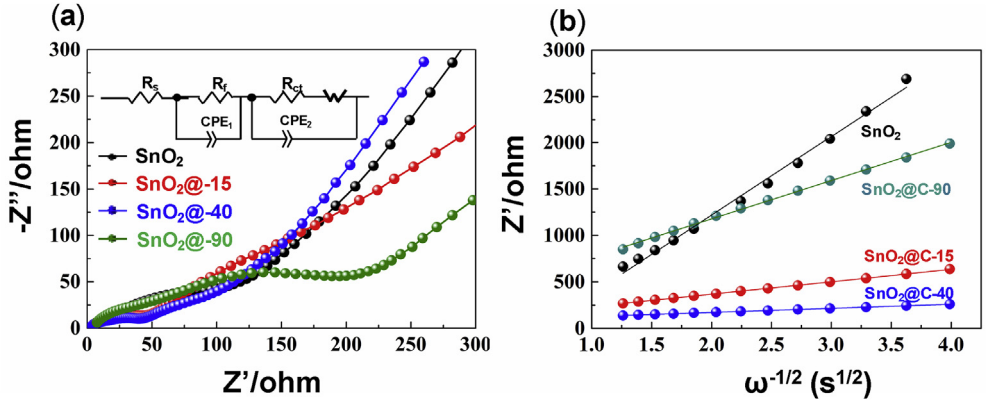

Fig. 8. Nyquist plot results (a) and illustrations of relationships between Z' and $\omega^{-1/2}$ in the low-frequency region (b). Thereinto, the R_s, R_f, R_{ct}, CPE_1, CPE_2 and Z_W belonging to the internal resistance, equivalent circuit fitting to the plots represent the contact resistance, charge-transfer impedance, constant phase element of the SEI film, constant phase element of the electrode-electrolyte interface and Warburg impedance, respectively.

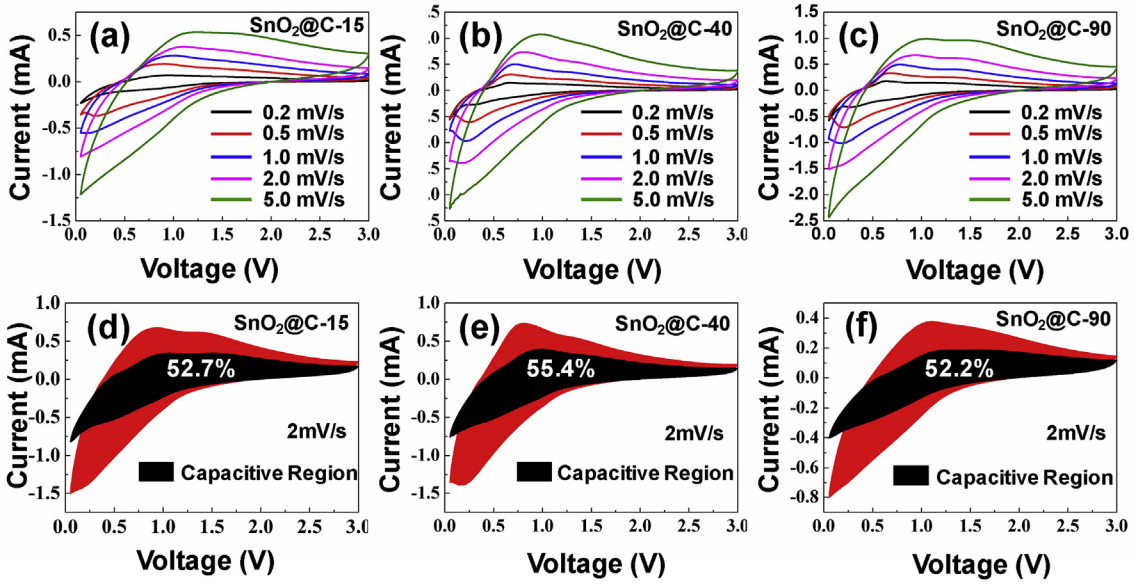

Fig. 9. The capacitive contributions in storage capacity of SnO_2@C-15, SnO_2@C-40 and SnO_2@C-90 are illustrated. Thereinto, (a), (b) and (c) are the CV measurement results at different scan rates. (d), (e) and (f) are the CV curves with capacitive fraction demonstrated by the shaded area at a scan rate of 2 mV/s.

the $NH_3 \bullet H_2O$ (4 M), gelatin as carbon source and $SnCl_4 \bullet 5H_2O$ as tin source is effective and facile way to fabricate SnO_2@C composite materials. Compared with the SnO_2, the SnO_2@C-40 composite materials show the more fabulous Li^+ storage capacity (397.7 mAh/g), after cycling charge-discharge 500 times. It is identified that controlling the carbon contents in SnO_2@C composite materials is pivotal factor to upgrade the Li^+ storage capacity. In storage mechanism, the pseudocapacitance effect that produced by microcrystalline structure of SnO_2 existing in the SnO_2@C composite materials plays the role to improve storage capacity. The possibility of SnO_2 as negative electrode materials in actual fabrication of LIBs is unveiled through our studies.

CRediT authorship contribution statement

Shangkun Wang: Experimenting, Writing – original draft. **Guiying Xu:** Investigation, Methodology. **Kun Wang:** Methodology, Investigation, Electrochemical evaluation. **Beibei Han:** Investigation, Measurement. **Yingxin Wang:** Advisor. **Lixiang Li:** Methodology. **Dongying Ju:** Supervision. **Maorong Chai:** Supervision. **Dakui Zhang:** Advisor, Experiment. **WeiMin Zhou:** Conceptualization, Writing – review & editing.

Declaration of competing interest

The authors declare that they have no known competing financial interests or personal relationships that could have appeared to influence the work reported in this paper.

Acknowledgements

We are grateful to the support of University of Science and Technology Liaoning (601009816–39) and 2017RC03. This work obtained the support by the Liaoning Province Education Department of China (Grant No.601009887–16). This work was partly supported with the project supported by the National Natural Science Foundation of China (Grant No. 51672117 and 51672118).

Appendix A. Supplementary data

Supplementary data to this article can be found online at https://doi.org/10.1016/j.crgsc.2021.100099.

References

[1] J.R. Dahn, T. Zheng, Y. Liu, X. Hu, Mechanisms for lithium insertion in carbonaceous materials, Science 270 (1995) 590–593.

[2] S.J. Yu, V.M.H. Ng, F.J. Wang, Z.H. Xiao, C.Y. Li, L.B. Kong, W.X. Que, K. Zhou, Synthesis and application of iron-based nanomaterials as anodes of lithium-ion batteries and supercapacitors, J. Mater. Chem. 6 (2018) 9332–9367.

[3] Y. Xu, K.J. Zhu, P.C. Liu, J. Wang, K. Yan, J.S. Liu, J. Zhang, J. Li, Z.R. Yao, Controllable synthesis of 3D Fe_3O_4 micro-cubes as anode materials for lithium ion batteries, CrystEngComm 21 (2019) 5050–5058.

[4] J.J. Zhou, T. Yang, M.L. Mao, W.L. Ren, Q.H. Li, Enhanced electrochemical performance of hierarchical $CoFe_2O_4/MnO_2$/C nanotubes as anode materials for lithium-ion batteries, J. Mater. Chem. 3 (2015) 12328–12333.

[5] Y.F. Deng, L.N. Wan, Y. Xie, X.S. Qin, G.H. Chen, Recent advances in Mn-based oxides as anode materials for lithium ion batteries, RSC Adv. 4 (2014) 23914–23935.

[6] X.Y. Liu, Y.L. Han, Q. Li, D. Pan, SnO_2 Nanoparticles for lithium-ion batteries prepared by sol-gel method, Key Eng. Mater. 727 (2017) 718–725.

[7] Y.Q. Guo, R.Q. Tan, Y. Li, W.J. Song, Solution route to SnO_2 crystals with controllable morphology, Appl. Surf. 258 (2012) 1958–1963.

[8] P. Roy, S.K. Srivastava, Nanostructured anode materials for lithium ion batteries, J. Mater. Chem. 3 (2015) 2454–2484.

[9] Y.N. Ko, S.B. Park, Y.C. Kang, Design and fabrication of new nanostructured SnO_2-carbon composite microspheres for fast and stable lithium storage performance, Small 10 (2014) 3240–3245.

[10] Q.H. Tian, Y. Tian, Z.X. Zhang, L. Yang, S.I. Hirano, Design and preparation of interconnected quasi-ball-in-ball tin dioxide/carbon composite containing void-space with high lithium storage properties, Carbon 95 (2015) 20–27.

[11] Y.H. Liu, X. Fang, M.H. Ge, J.P. Rong, C.F. Shen, A.Y. Zhang, H.A. Enaya, C.W. Zhou, Single-step flash-heat synthesis of red phosphorus/graphene flame-retardant composite as flexible anodes for sodium-ion batteries, Nano Research 11 (2018) 3780–3790.

[12] Z.L. Wang, D. Xu, H.X. Zhong, J. Wang, F.L. Meng, X.B. Zhang, Gelatin-derived sustainable carbon-based functional materials for energy conversion and storage with controllability of structure and component, Science adv 1 (2015), e1400035.

[13] M. Lian, J.C. Fan, Z.X. Shi, S. Zhang, H. Li, J. Yin, Gelatin-assisted fabrication of graphene-based nacre with high strength, Carbon 89 (2015) 279–289.

[14] J.K. Li, G.Y. Xu, K. Wang, B.B. Han, L.X. Li, Y.X. Wang, D.Y. Ju, M.R. Chai, D.K. Zhang, W.M. Zhou, Study on fabrication and electrochemical performances of Fe_7S_8@C composite materials, Electrochemistry 88 (2020) 380–386.

[15] D. Mohanta, M. Ahmaruzzaman, Tin oxide nanostructured materials: an overview of recent developments in synthesis, modifications and potential applications, RSC Adv. 6 (2016) 110996–111015.

[16] B. Liu, M.H. Cao, X.Y. Zhao, Y.C. Tian, W. Hu, Facile synthesis of ultrafine carbon-coated SnO_2 nanoparticles for high-performance reversible lithium storage, J. Power Sources 243 (2013) 54–59.

[17] W.W. Xu, X.D. Cui, Z.Q. Xie, G. Dietrich, Y. Wang, Three-dimensional coral-like structure constructed of carbon-coated interconnected monocrystalline SnO_2 nanoparticles with improved lithium-storage properties, ChemElectroChem 3 (2016) 1098–1106.

[18] J. Liu, L.T. Yu, C. Wu, Y.R. Wen, K.B. Yin, F.K. Chiang, R.Z. Hu, J.W. Liu Jw, L.T. Sun, L. Gu, J. Maier, Y. Yu, M. Zhu, New nanoconfined galvanic replacement synthesis of hollow Sb@C yolk–shell spheres constituting a stable anode for high-rate Li/Na-ion batteries, Nano Lett. 17 (2017) 2034–2042.

[19] H.Y. Lu, Y.X. Wan, T.Y. Wang, R. Jin, P.T. Ding, R. Wang, Y. Wang, C. Teng, L.L. Li, X.L. Wang, D.S. Zhou, G. Xue, A high performance SnO_2/C nanocomposite cathode for aluminum-ion batteries, J. Mater. Chem. 7 (2019) 7213–7220.

[20] P.F. Tian, Y.H. Wang, W. Li, S.W. Song, S.Y. Zhou, H.W. Gao, H.Q. Xu, X.Q. Tian, J.B. Zang, A salt induced gelatin crosslinking strategy to prepare Fe-N doped aligned porous carbon for efficient oxygen reduction reaction catalysts and high-performance supercapacitors, J. Catal. 382 (2020) 109–120.

[21] J. Niu, J.J. Liang, A. Gao, M.L. Dou, Z.P. Zhang, X. Lu, F. Wang, Micropore-confined amorphous SnO_2 subnanoclusters as robust anode materials for Na-ion capacitors, J. Mater. Chem. 7 (2019) 21711–21721.

[22] S.L. Zhang, J.H. Zhang, G.Q. Cao, Q. Wang, J.H. Hu, P. Zhang, G.S. Shao, Strong interplay between dopant and SnO_2 in amorphous transparent (Sn, Nb) O_2 anode with high conductivity in electrochemical cycling, J. Alloys Compd. 735 (2018) 2401–2409.

[23] X.Y. Li, L.P. Xiao, L. Zhou, Q.C. Xu, J. Weng, J. Xu, B. Liu, Adaptive bifunctional electrocatalyst of amorphous CoFe Oxide@2D black phosphorus for overall water splitting, Angew. Chem. Int. Ed. 59 (2020) 21106–21113.

[24] X.Y. Zhu, Z.H. Zhang, Y. Mao, Y. Li, X. Huang, N. Gu, Applying deep learning in automatic and rapid measurement of lattice spacings in HRTEM images, Sci. China Materials 63 (2020) 2365–2370.

[25] X.M. Yang, A.L. Rogach, Electrochemical techniques in battery research: a tutorial for nonelectrochemists, Adv. Energy Mater 9 (2019) 1900747.

[26] J.B. Wang, Z.W. Liu, W.J. Yang, L.J. Han, M.D. Wei, A one-step synthesis of porous V_2O_3@C hollow spheres as a high-performance anode for lithium-ion batteries, Chem. Can. 54 (2018) 7346–7349.

[27] H.R. Du, K.F. Huang, W. Dong, B.Y. Geng, A general gelatin-assisted strategy to hierarchical porous transition metal oxides with excellent lithium-ion storage, Electrochim. Acta 279 (2018) 66–73.

[28] A.P. Wang, S. Kadam, H. Li, S.Q. Shi, Y. Qi, Review on modeling of the anode solid electrolyte interphase (SEI) for lithium-ion batteries, NPJ Comput. Mater 4 (2018) 1–26.

[29] K. Kisu, M. Iijima, E. Iwama, M. Saito, Y. Orikasa, W. Naoi, K. Naoi, The origin of anomalous large reversible capacity for SnO_2 conversion reaction, J. Mater. Chem. A. 2 (2014) 13058–13068.

[30] M. He, L.X. Yuan, X.L. Hu, W.X. Zhang, J. Shu, Y.H. Huang, A SnO_2@carbon nanocluster anode material with superior cyclability and rate capability for lithium-ion batteries, Nanoscale 5 (2013) 3298–3305.

[31] L.L. Fan, X.F. Li, B. Yan, J.M. Feng, D.B. Xiong, D.J. Li, L. Gu, Y.R. Wen, S. Lawes, X.L. Sun, Controlled SnO_2 crystallinity effectively dominating sodium storage performance, Adv. Energy Mater 6 (2016) 1502057.

[32] J.J. Wang, L.Y. Wang, S.Y. Zhang, S.Y. Liang, X.Q. Liang, H.F. Huang, W.Z. Zhou, J. Guo, Facile synthesis of iron-doped SnO_2/reduced graphene oxide composite as high-performance anode material for lithium-ion batteries, J. Alloys Compd. 748 (2018) 1013–1021.

[33] X.M. Lou, C.F. Lin, Q. Luo, J.B. Zhao, B. Wang, J.B. Li, Q. Shao, X.K. Guo, N. Wang, Z.H. Guo, Crystal structure modification enhanced $FeNb_{11}O_{29}$ anodes for lithium-ion batteries, ChemElectroChem 4 (2017) 3171–3180.

[34] C.F. Lin, L. Hu, C.B. Cheng, K. Sun, X.K. Guo, Q. Shao, J.B. Li, N. Wang, Z.H. Guo, Nano-$TiNb_2O_7$/carbon nanotubes composite anode for enhanced lithium-ion storage, Electrochim. Acta 260 (2018) 65–72.

[35] B. Liu, X.Y. Zhao, Y. Xiao, M.H. Cao, High-surface-area F-doped amorphous MoO_x with high-performance lithium storage properties, J. Mater. Chem. 2 (2014) 3338–3343.

[36] R.Z. Zhao, Z. Qian, Z.Y. Liu, D.Y. Zhao, X.B. Hui, G.Z. Jiang, C.X. Wang, L.W. Yin, Interface-coupling in FeOOH/MXene heterojunction for highly reversible lithium-ion storage, Materials Today Energy 19 (2021) 100584.

[37] J. Wang, J. Polleux, J. Lim, B. Dunn, Pseudocapacitive contributions to electrochemical energy storage in TiO_2 (anatase) nanoparticles, J. Phys. Chem. C 111 (2007) 14925–14931.

[38] D.L. Chao, C.R. Zhu, P.H. Yang, X.H. Xia, J.L. Liu, J. Wang, X.F. Fan, S.V. Savilov, J.Y. Lin, H.J. Fan, Z.X. Shen, Array of nanosheets render ultrafast and high-capacity Na-ion storage by tunable pseudocapacitance, Nat. Commun. 7 (2016) 12122.